Type of the Paper (Article)

Proton detected solid-state NMR of membrane proteins at 28 Tesla and 100 kHz magic-angle spinning

Evgeny Nimerovsky[1], Kumar Tekwani Movellan[1], Xizhou Zhang[1], Marcel C. Forster[1], Eszter Najbauer[1], Kai Xue[1], Rıza Dervişoğlu[1], Karin Giller[1], Christian Griesinger[1], Stefan Becker[1], Loren B. Andreas[1]*

[1] NMR-based Structural Biology, Max-Planck-Institute for Biophysical Chemistry, Göttingen, Germany
* Correspondence: land@nmr.mpibpc.mpg.de.com; Tel.: +49 551 201-2214

Abstract: The available magnetic field strength for high resolution NMR in persistent superconducting magnets has recently improved from 23.5 to 28 Tesla, increasing the proton resonance frequency from 1 to 1.2 GHz. For magic-angle spinning (MAS) NMR, this is expected to improve resolution, provided the sample preparation results in homogeneous broadening. We compare two-dimensional (2D) proton detected MAS NMR spectra of four membrane proteins at 950 and 1.2 GHz. We find a consistent improvement in resolution that scales superlinearly with the increase in magnetic field for three of the four examples. In 3D and 4D spectra, which are now routinely acquired, this improvement indicates the ability to resolve at least 2 and 2.5 times as many signals, respectively.

Keywords: magic-angle spinning; solid-state NMR; membrane protein; beta barrel; transmembrane; proton detection; high magnetic field;

1. Introduction

Protons not only have a high gyromagnetic ratio, but are also abundant in biological molecules, making them an ideal choice for detection.[1, 2] Although this does indeed maximize sensitivity when defining sensitivity in terms of peak area, in solid samples the many strong proton-proton dipole couplings lead to broad spectra at magic-angle spinning (MAS) frequencies of below ~20 kHz[3] unless significant proton dilution is employed.[4-9] For proteins, the most common approach has been to perdeuterate during expression, and then introduce the protein to the desired concentration of H_2O in D_2O in order to reintroduce protons at exchangeable sites at a defined level. This works efficiently for most proteins, but becomes problematic for some membrane proteins due to the lack of exchange for the membrane embedded regions.[10, 11] So far, the sample preparation has been the major bottleneck limiting the number of ssNMR studies of membrane proteins. Indeed, their expression yields are often particularly limited in perdeuterated media, and sidechain information is limited. Although improved resolution is observed with lower levels of protons at exchangeable sites, this only partly compensates for a loss in sensitivity.[12, 13]

A complementary strategy to proton dilution is to increase the MAS frequency[14-16] and the magnetic field in order to reduce spin relaxation occurring via spin flip-flops.[17, 18] This places less stringent demands on proton dilution[19-22] and results in high sensitivity despite a reduction in sample amount to only 2 to 3 mg for 1.3 mm rotors spun up to 60 kHz MAS, as recently reviewed.[23] Further increases in the MAS have resulted in improved sensitivity per unit of sample, with 0.8 mm and 0.7 mm probes that deliver a spinning frequency over 100 kHz. It is not yet clear which MAS frequency will be found to be optimal, and indeed recent reports of a 0.6 mm probe indicate further improvement in relaxation properties at 126 kHz MAS leading to an average proton linewidth < 100 Hz.[24]

Tailored isotopic labeling of side chain protons is more challenging, relying on control of labeling during protein expression, which depends on the expression media, but also on metabolic processes of the expression system. The group of Reif realized that the conditions used for perdeuterated protein expression results in approximately 10 percent CHD_2 labeling of methyl sites and leads to spectacular resolution of side chain proton resonances.[8, 25] The strategy can be improved by use of a methyl precursor and optimization of the level of H_2O during expression. [26] Generalization of side chain labeling via expression in deuterated glucose or glycerol with defined H_2O levels was dubbed Reduced Adjoining Protonation (RAP), and allowed detection at all side chain sites.[27-29] A related approach, fractional deuteration (FD) involves the use of protonated glucose in an otherwise deuterated expression medium. Protonation levels are 10 to 40 percent, with the alpha proton labeling sourced primarily from the water.[30]
Metabolic precursors developed for labeling in solution provided an appealing approach to improve side labeling efficiency in a deuterated background.[31-35] Methyl protons can provide valuable information that defines the protein fold.[34, 36] Stereo-Array Isotope Labeling (SAIL) provides further control of protonation, and for Valine, leads to reduction of proton linewidths by a factor of 2 to 7.[37] The high cost of SAIL can be offset by the use of smaller rotors.[38] For alpha proton labeling, alpha proton exchange via transamination (αPET) leads to improved linewidths at 55-100 kHz, albeit with scrambling of the label for certain residue types.[39]
Full protonation is by far the most straightforward approach, which even allows expression in insect[40, 41] or mammalian media.[42] Several reports first proposed the detection of side-chain protons in the 40 to 60 kHz regime,[43-45] but the relatively low resolution for fully protonated samples in this spinning range limits applications. The development of 0.7 mm probes capable of spinning above 100 kHz led to a resolution improvement that has expanded applications to structure determination of proteins, and analysis of materials without isotopic enrichment.[46-49]

Nevertheless, it is clear that further increase in both the spinning frequency and the magnetic field could improve proton resolution, in particular for strongly coupled spins with similar frequencies.[50] A theoretical framework for efficient line shape calculation involving many spins was applied recently to proteins.[51] Restricted state-space simulations also can be used to simulate large spin clusters necessary for accurate linewidth determination.[52, 53] Such simulations apply to rigid systems, and when dynamics are present, additional sources of spin relaxation exist.[54]

The presence of dynamical processes is a well-known phenomenon in membrane proteins.[55] Furthermore, the sample homogeneity in membrane bilayer preparations of membrane proteins is often less ideal than microcrystalline or sedimented proteins, for which several detailed reports have already investigated the effects of magnetic field and spinning frequency for protonated and partly deuterated proteins.[28, 44] Particularly narrow lines similar to microcrystalline preparations were reported for the membrane protein bacteriorhodopsin,[56] an apparent exception to the usual situation.

The recent installation of 28 Tesla magnets provides an opportunity to quantify the expected improvements in resolution and sensitivity as observed in MAS spectra. Are the spectra characterized by mainly inhomogeneous broadening, in which case similar spectral quality can be expected? Or are membrane protein spectra more often characterized by homogeneous effects that are expected to either scale down with field (coherent effects) or remain more or less the same (incoherent effects)?

We approach this topic by presenting proton detected spectra of four membrane proteins, two helical proteins, the matrix protein 2 (M2) from influenza A and a citrate sensor (CitA) from *Geobacillus Thermodenitrificans* and two beta

barrels, the human voltage dependent anionic channel (hVDAC) and opacity associated protein 60 (Opa60) from *Neisseria Gonorrhoeae*. In each case, we compare the spectra taken from a single fully-protonated sample packed in a 0.7 mm rotor and recorded at a 950 MHz spectrometer, and at a 1.2 GHz spectrometer.

2. Materials and Methods

NMR spectroscopy:

Measurements at 950 MHz were recorded using a Bruker Avance III HD spectrometer equipped with a 0.7 mm HCDN MAS probe using 156 kHz proton, 80 kHz carbon and 35 kHz nitrogen rf-fields for hard pulses. Measurements at 1200 MHz were recorded using a Bruker Avance NEO spectrometer equipped with a 0.7 mm HCN prope using 144 kHz proton, 83 kHz carbon and 78 kHz nitrogen rf-fields for hard pulses. All spectra were recorded at 100 kHz MAS using cooling gas flow of 500 lph and a temperature of 260 to 265 K to maintain a sample temperature near 288 K. For all spectra 25 kHz MISSISSIPPI[57] water suppression (100 to 200 ms), 23 kHz Swf-TPPM proton decoupling during acquisition of the indirect dimension and 10 kHz WALTZ-16 heteronuclear decoupling during acquisition was employed. Spectra were processed in Bruker topspin versions 3 and 4, and analyzed in Sparky.[58]

Drift in the magnetic field was compensated in processing with linear drift correction using a script directly in Topspin. was applied for the 1.2 GHz (H)NH spectrum. [59] This was particularly important for Opa60 spectra at the 1.2 GHz, since data acquisition took place in the first few weeks after charging, and the magnet was still drifting at over 200 Hz per hour, and the drift rate was changing every day. Details of the acquisitions including CP transfer parameters are summarized in Tables S1 and S2 in the SI.

For linewidth determination, no apodization was used, and the time domain signal was sampled far enough (>3 times T_2) to minimally impact the linewidth determination. For example, for Opa60, spectra from both spectrometers were sampled in the proton dimension to 9.1 ms, and for nitrogen linewidth analysis, 12.5 ms nitrogen sampling was used at 1.2 GHz and 15.75 ms for the 950 MHz spectra, ensuring a valid comparison in ppm, and >3 times T_2 for the narrowest signal identified.

M2:

The conductance domain construct (residue 18 to 60) of M2 with a C50S mutation was expressed in ^{13}C,^{15}N labeled form and reconstituted in DPhPC membranes as previously reported.[60] Briefly, the expression of the M2 construct containing a TrpLE followed by a 6xHis C-terminal tag was performed in minimal media supplemented with ^{13}C-glucose, ^{15}N-NH4Cl and centrum vitamins using *Escherichia Coli* (BL21-DE3). After cell disruption the inclusion bodies containing the ^{13}C,^{15}N-M2 fusion protein were pelleted by centrifugation and resuspended in 6M guanidinium hydrochloride. The solubilized protein was passed through a nickel column. The elution fractions containing protein were dialyzed against H_2O and lyophilized. The lyophilized protein was cleaved with cyanogen bromide, purified by HPLC, and lyophilized. For membrane reconstitution, the lyophilized protein was resuspended in NMR buffer containing octyl glucoside and mixed with d_{78}-phytamoyl, d_9-choline lipids (from FBReagents) using 1 to 1 lipid to protein mass ratio. The detergent was removed by dialysis. The sample was pre-packed in a 1.3 mm rotor and then transfer to a 0.7 mm rotor.

CitA:

The uniformly ^{13}C, ^{15}N labeled Gt CitApc sample with C12A and R93A mutations was expressed and purified using a previously published protocol.[61] The protein was finally reconstituted into a mixture of 1,2-dimyristoyl-sn-glycero-3-phosphocholine (DMPC) and 1,2-dimyristoyl-sn-glycero-3-phosphatic acid (DMPA) liposomes (with DMPC to DMPA molar ratio of 9:1). The protein to lipid molar ratio was 1:75. The liposome sample was pelleted by ultracentrifugation and suspended into buffer at pH 6.5 with 20 mM sodium phosphate and 5mM

sodium citrate. To get the citrate bound state, 5mM sodium citrate was supplemented during all purification steps. The sample was pre-packed in a Bruker 1.3 mm rotor and then transferred to a 0.7 mm rotor by ultracentrifugation.

VDAC:

The α-PET hVDAC1 sample was prepared as described in before.[39] Briefly, the c-terminally histidine tagged protein was expressed to inclusion bodies in *Escherichia Coli* BL21 DE3 cells, purified via affinity, refolded, and finally purified by size exclusion chromatography. 2D crystalline preparations in DMPC lipids were prepared as previously described. [62]

Opa60

A protocol for purification of Opa60 has been published earlier [63] and we recently used this protocol as the basis for reconstitution in lipid bilayers.[64] Briefly, uniform ^{13}C,^{15}N-labeled Opa60 with a C-terminal histidine affinity tag was expressed in *Escherichia coli* BL21(DE3) in M9 medium. After harvesting, cells were lysed by sonication. Inclusion bodies, consisting of Opa60, were purified by centrifugation, and subsequently solubilized in guanidinium hydrochloride. Solubilized protein was further purified using Ni^{2+} affinity chromatography. Opa60 was then refolded by 40-fold dilution into a buffer containing 0.25% dodecylphosphocholine (DPC). Refolded protein was purified using gel filtration. Opa60 was reconstituted into lipid bilayers consisting of deuterated DMPC (Avanti Polar Lipids) by dialysis with a lipid-to-protein mass ratio of 0.25. The final sample was packed into a Bruker 0.7 mm rotor.

Simulations:

The numerical simulations shown in Fig. 7 were performed using in-house MATLAB scripts, solving the equation of motion.[65] with the previous described method.[66] The total Hamiltonian of N spins consisted of the sum of the N isotropic chemical shift Hamiltonians and 0.5*N*(N-1) homonuclear dipolar Hamiltonians. The distances and the relative orientations of the different Principal Axis systems of the dipolar interactions with respect to molecular frame were calculated according to the coordinates in the pdb 2N70, as detailed in the SI. In calculations, the dipolar interactions between methyl protons was averaged by 3 because of the inner rotation of the group.[67] The initial and the measured operators were I^+ and I^-, respectively. For measuring the full width of the peaks at half maximum (FWHM), the simulated signal was multiplied by a mono-exponential function corresponding 32 Hz FWHM for Fig. 7 A-E, and 16 Hz for the angle dependence of Fig. 7F, for which 16 Hz was used. Time domain simulations were transferred into the frequency domain with the Fourier transform. The illustration of the selected proton spins is shown in the supplemental information Fig. S1.

Structural refinement and NMR chemical shift calculations with DFT:

Density functional theory (DFT) calculations were performed using gaussian 16 software.[68] As starting structures, we used the protein database (pdb) 2N70 and 6BKL and introducing an H_2O molecule next to residue G34 inside the tetramer structure of the protein. To accelerate the DFT and Gauge-Independent Atomic Orbital (GIAO)[69] based NMR calculations, a reduced set of atoms spanning residues I33 to W41, were used. Two starting structures were optimized with first semi-empirical and later DFT methods using different functionals (hybrid and HF)[70] and basis sets available in Gaussian16. The structures were optimized stepwise, first by a semi-empirical PM6[71] and later by hybrid B3LYP[72] or pure Hartree-Fock (HF)[70] level of theory with 6-311G++2d,p for B3LYP and 6-31G for HF as basis sets. After addition of the water molecule next to G34, the structures were reoptimized before performing the NMR calculations using the GIAO method. The proton chemical shift is calculated using TMS (31.882 ppm) as reference for protons from the chemical shielding tensor of the GIAO results. We observe a correlation coefficient R^2 of 0.98 for assigned proton resonances of the selected residues.

3. Results and Discussion

Substantial improvement in resolution is observed at 1.2 GHz, which is generally better than a linear linewidth reduction in ppm as compared with the 950 MHz data. An improvement in sensitivity for the (H)NH and (H)CH spectra of about 1.3 ± 0.5 is observed as compared with the 950 MHz instrument, consistent with the expected $B_0^{1.5}$ dependence. The large variation emphasizes the importance of carefully optimizing the RF pulses and cross polarization transfer steps, and the need for a better proton sensitivity standard for MAS NMR.

3.1 M2

The M2 protein from Influenza A is a small viroporin that is the target of two adamantane-based drugs,[73] and for which development of additional inhibitors is of interest.[74] Figure 1 shows a comparison of 2D (H)NH and (H)CH spectra of the 18-60 construct of M2 in 1,2-diphytanoyl-*sn*-glycero-3-phosphocholine (DPhPC) lipid bilayers.[60] To evaluate the improvement in spectral resolution, we selected several isolated peaks and compared the proton linewidths. A consistent reduction in the linewidths in Hz is observed, indicating an improvement in resolution that exceeds the ratio of the magnetic fields. For example, for the selected amide protons, the improvement ranges from a factor of 1.3 to 1.5, while the ratio of fields is 1.26.

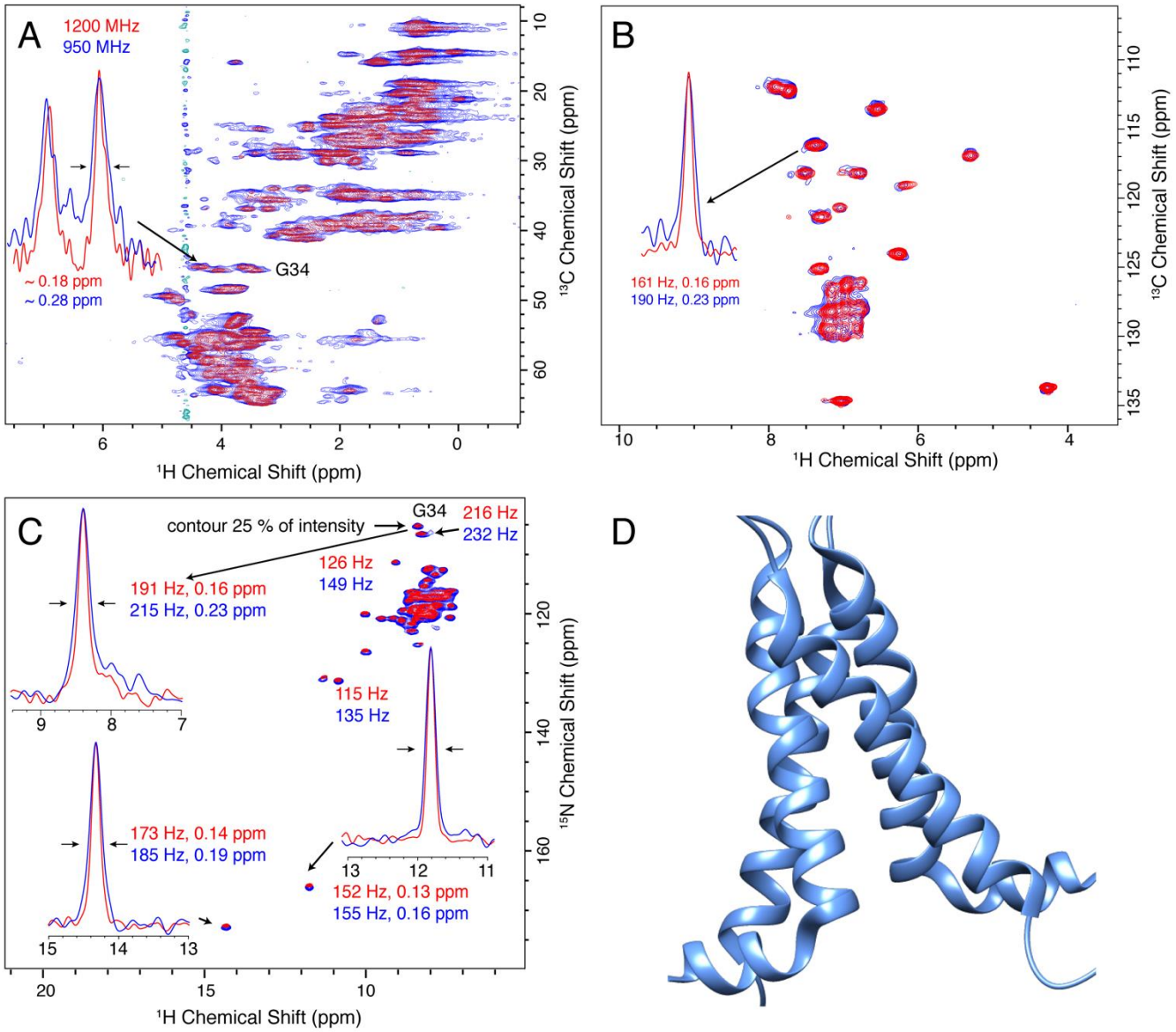

Figure 1. Spectra of fully protonated Influenza A M2 at recorded at 950 (blue) and 1200 (red) MHz spectrometers using 100 kHz MAS. Panel (A) shows the CP based C-H spectrum, (H)CH, and the slice shows linewidths of G34 α protons. In (B), the aromatic region of the same spectrum is shown. Panel (C) shows the CP based N-H spectrum and linewidths of selected peaks. In (D), the tetrameric structure of M2 is shown, taking the coordinates from protein data bank (PDB) code 2N70, which contains the S31N substitution, but shows a similar 'dimer-of-dimers' spectrum as the wild type sequence for which the spectra were recorded.

3.2 CitA

The histidine kinase CitA senses citrate on the outside of the bacterial inner membrane, which triggers an intracellular response. A construct containing the sensor domain (PASp), both transmembrane helices (TM1 and TM2), and the cytosolic PASc domain contains the key elements to study transmembrane signaling.[61] It contains both alpha helical and beta sheet components outside the membrane, and two transmembrane helices. 100 kHz MAS spectra at both 950 MHz and 1200 MHz are shown in Figure 2A-C, and a cartoon showing the topology of the protein is shown in panel D. Similar to the M2 spectra, proton resolution is improved by 20 to 60 Hz at 1.2 GHz as compared with the 950 MHz spectra, resulting in linewidths of 0.1 to 0.15 ppm.

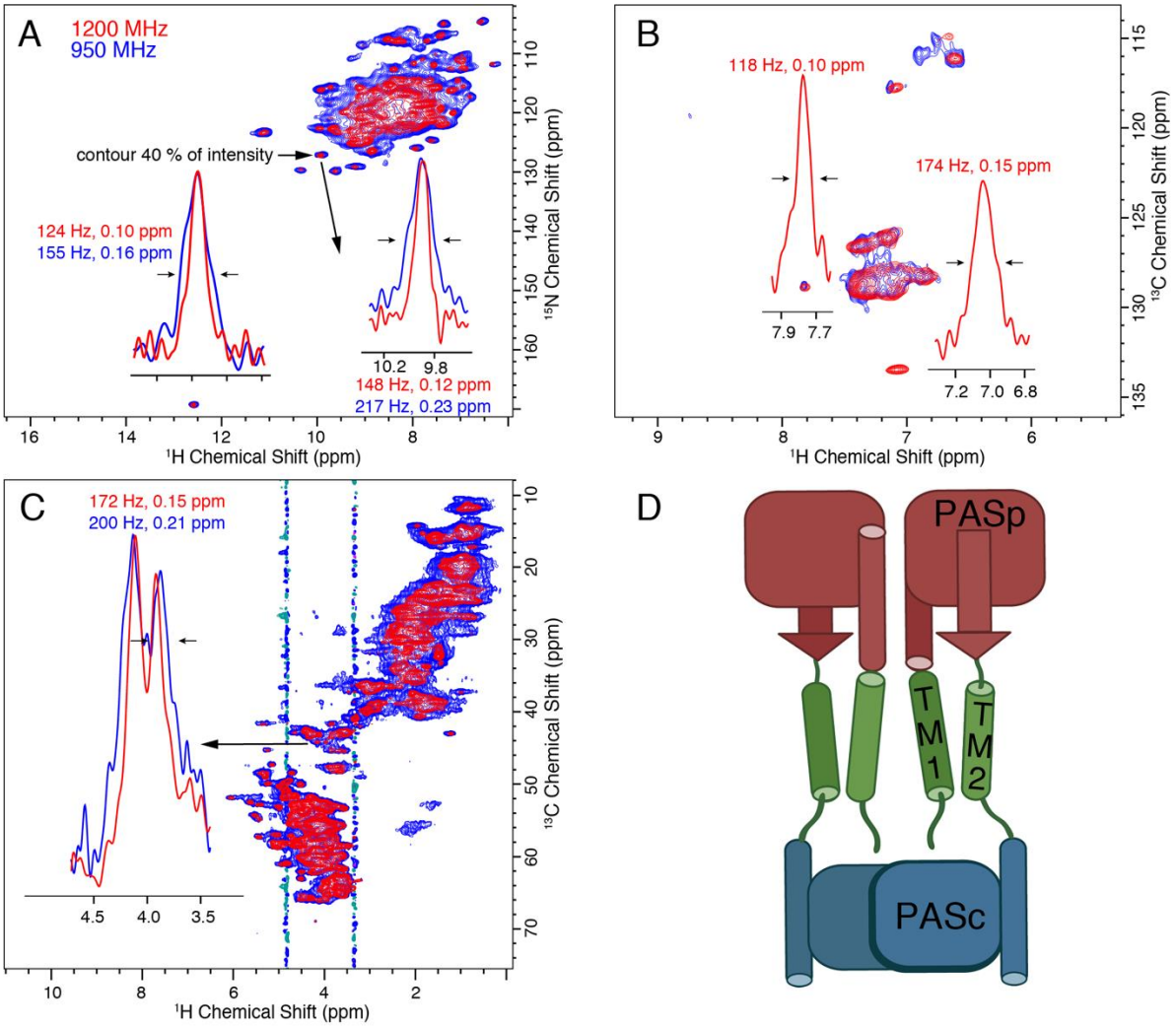

Figure 2. Resolution and sensitivity of CitApc (H)NH and (H)CH spectra are improved using the 1.2 GHz instrument (red) as compared with the 950 MHz (blue). The resulting improvement in peak separation is evident in both the (H)NH (A) and (H)CH (B) spectra. This is especially obvious in the glycine region of the (H)NH spectra below 110 ppm. 1D proton traces (inset in A, B and C) reveal the resolution improvement of various isolated peaks. The aromatic

carbon region of the (H)CH spectrum (B) has a higher sensitivity using the 1.2 GHz magnet, such that linewidths could only be measured at 1.2 GHz. The topology of the protein is shown in D with the sensor PASp domain in red, the transmembrane helices (TM1 and TM2) shown in green, and the PASc domain shown in blue.

3.3 VDAC

The human voltage dependent anion channel (hVDAC) is a 19-stranded beta barrel that mediates metabolite flux across the outer mitochondrial membrane. Preparations where 2D lipid crystalline arrays can be observed in negative stain electron micrographs result in particularly well resolved spectra.[62, 75] Figure 3 shows the proton detected spectra of an α-PET labeled sample of the 32 kDa membrane protein hVDAC. The α-PET labeling results in a substantial degree of side-chain deuteration, such that we expect a narrower proton linewidth as compared with full protonation. Indeed, in the case of hVDAC, we observe that both proton and heteronuclear linewidths stay the same in Hz between the 950 and 1200 MHz instruments, leading to 20% narrower linewidths on the ppm scale. The (H)NH spectrua are compared in panel A, and the (H)CH spectra of panel B demonstrate the suppression of most side-chain proton resonances using α-PET labeling. The high resolution structure (pdb 3EMN) is shown in C.

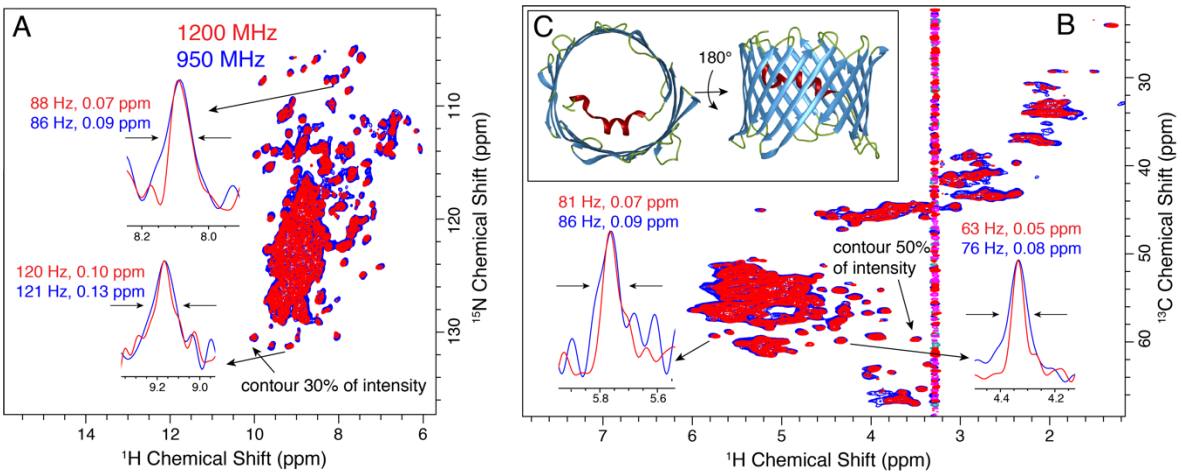

Figure 3: Improved resolution of 2D crystalline α-PET hVDAC at 1200 MHz (red) compared with 950 MHz (blue). A and B show the (H)NH and (H)CH spectra, respectively. The inlays show the improvement in line widths on the ppm scale for proton. C Shows the 3D structure of VDAC (pdb: 3EMN). α-helical regions are shown in red, β-strands in blue, loops in green.

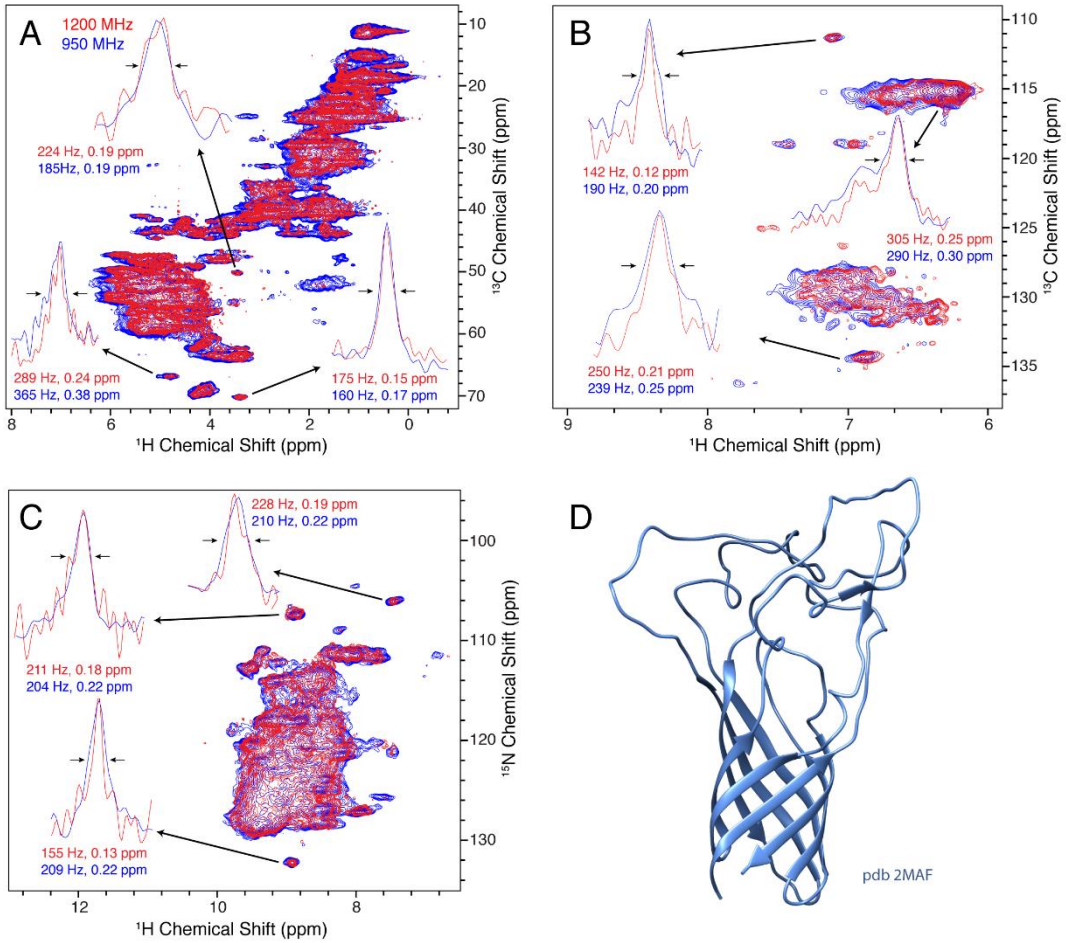

Figure 4. Resolution of the beta barrel protein Opa60 at 1200 MHz (red) and 950 MHz (blue). A, B, and C, show the aliphatic (H)CH, aromatic (H)CH, and (H)NH spectra, respectively. The insets show the linewidths of selected peaks that are resolved in the 2D spectrum. In D, the solution structure (pdb 2MAF) is shown.

3.4 Opa60

Opa60 is a member of the Opa (Opacity-associated) family of proteins found in the bacterial pathogens *Neisseria gonorrhoea* and *N. meningitidis*.[76] During infection, they mediate the adhesion to and uptake into human host tissues.[77] Opa60 is a 28 kDa beta-barrel transmembrane protein. with eight individual strands spanning the outer bacterial membrane. The large extracellular loops confer receptor specificity and differ in between different Opa variants. [76, 78] The structure of Opa60 has been determined by solution-state NMR in detergent micelles,[63] but no structure in lipid bilayers has been reported to date. Structure determination of Opa60 in lipid bilayers holds the potential of assessing this question in a physiologically meaningful manner. For Opa60, we find that after correcting for the different recycle delays used on the spectrometers, the sensitivity stays roughly the same (signal-to-noise ratio of 0.9 for (H)NH, 1.0 for (H)CH). However, the final CP transfer before detection was shorter for both spectra on the 1.2 GHz machine, thus rendering our calculations a lower boundary for sensitivity improvement. Proton linewidths as shown in Figure 4A are generally comparable when measured in Hz, but decrease as expected when expressed in ppm.

In the above sections we compared the proton linewidth, since the protons have the strongest homonuclear couplings that are a major source of broadening in protein spectra. Although this source of broadening is absent from nitrogen and carbon spectra, it is also interesting to compare the resolution as a function of magnetic field. It is not immediately obvious if the lines are inhomogeneous and expected to remain the same with higher field, or homogeneous in which

case we may hope for an improvement in linewidth as measured in ppm. The situation, of course, depends upon the particular sample being studied. We find that for three of the four samples, a clear improvement in the nitrogen and carbon resolution is observe at 1.2 GHz (Figure 5), which is equal to or better than the ratio of magnetic fields, 1.26. The source of the observed improvement in the ^{15}N linewidth as measured in Hz is unclear. However, we have noted that the ^{15}N linewidth of fully protonated samples is also highly sensitive to the magic angle setting. The fourth protein, Opa60, showed a reduced improvement, as measured in ppm. This is explained by a larger inhomogeneous contribution to the line, and to a limited extent could also be due to the strong field drift of the 1.2 GHz instrument, which invariably has a small nonlinear component after charging the magnet. The linear component of the drift was removed using a drift correction script in TopSpin.[59] For 3 of the 4 membrane protein samples tested, we observe an improvement in resolution that is either better or equal to the ratio of fields, which is 1.26. Since the resolvability scales as the product of the improvement in each dimension, this indicates an expected improvement in resolvability that is better than 2 for 3D spectra, and above 2.5 for 4D spectra. A summary of the proton linewidth improvement is shown in Figure 6.

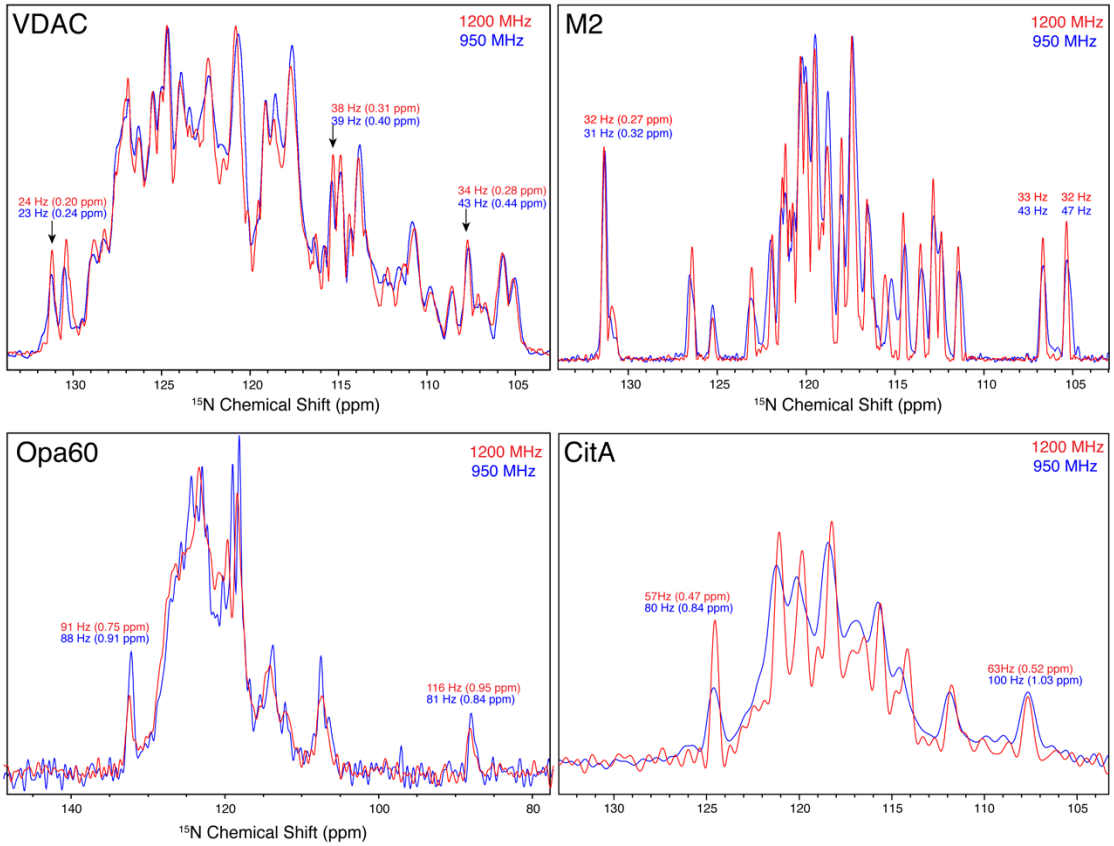

Figure 5. Nitrogen linewidths of the four proteins. Red spectra are from the 1200 MHz instrument, while blue spectra were recorded a 950 MHz. The proteins are indicated in the top left of each panel, VDAC, M2, Opa60, and CitA.

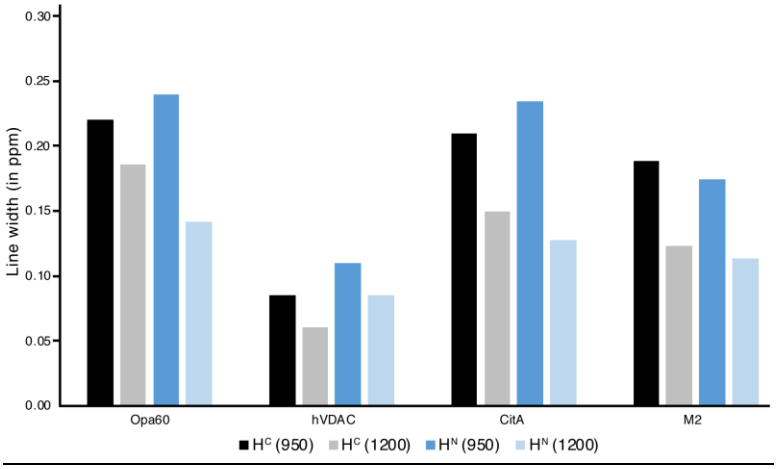

Figure 6. Average proton linewidth for the four membrane proteins, Opa60, hVDAC, CitA, and M2.

3.5 Proton Linewidth Simulations

In MAS NMR spectra, the proton linewidth is determined primarily from the influence of many strong proton-proton dipolar couplings, which are not completely averaged by the MAS. These linewidths can be simulated by solution of the equation of motion using numerical methods for up to about 10 spins.[51, 79] It was recently shown that a better determination of linewidths in ubiquitin required additional spins, and a second moment approach captures the behavior for rigid parts of the protein.[51] Here for simplicity, we chose a numerical approach using up to 12 spins, from which we can observe the trends in linewidth when spinning frequency or magnetic field are varied. Similar simulations for 3 to 4 spins are found in Asami et al.[28]

Figure 7 shows the simulated linewidth of the three protons of glycine, including up to 12 spins in the simulation, and over a range of magnetic fields and either at the magic angle ($\Delta\theta_R$=0) or with deviations up to ± 0.075° (Fig. 7 F). The 12 spins in the simulation were selected based on the alpha helical conformation near G34 of M2 from pdb 2N70, taking the closest protons. With 12 spins, the linewidth determination has not completely converged, but reaches about 80 percent of the measured values. Since the results are quite sensitive to exact coordinates and chemical shifts, the main point of the figure is to observe the trends with spinning frequency and magnetic field. The simulated amide linewidth of 161 Hz (Fig. 7A) can be compared with the measured value of 191 Hz (Fig. 1C). For the glycine alpha protons, the difference is much larger, with simulated linewidths of ~75 Hz that are far from the measured ~216 Hz (Fig 1A). Any magic angle misset during the measurement would bring the agreement closer, but not enough to bring the numbers into agreement (see below). The geometry of most of the closest spins is well defined by the alpha helical structure of the protein.

However, looking at the structure 2N70, there is a void near the G34 alpha protons, that would certainly be filled by either water or a sidechain of a neighboring helix, since there is still uncertainty in the solid-state NMR structure. Adding two protons to this void, representing water or methylene protons, results in better agreement (Fig. 7B-C) both for the amide and particularly for the alpha protons, emphasizing the sensitivity of the linewidth simulations to the arrangement of spins. Different chemical shifts were entered for the additional protons, for B and C, as detailed in the supporting information. Since the chemical shifts of these added protons are unknown, we first performed the simulations setting the isotropic shifts to 4.6 ppm. For comparison, we also simulated for the case of 3.2 and 2 ppm, which is the result of a DFT calculation in which a water molecule is added near G34. Note that these values are typical of aliphatic protons, such that this also represents the case of a nearby protein sidechain. A strong dependence of the aliphatic linewidths is observed between B and C, emphasizing the importance of the isotropic shifts in simulations. For panels A-E, a natural linewidth of 32 Hz was assumed. Fig. 7 D and E show the influence of magnetic

field for selected MAS frequencies, in Hz and in ppm, respectively. The improvement with increasing magnetic field becomes particularly evident when viewed on the ppm scale, which is what matters for resolution.

Commercial probes have been found to reach an accuracy of about 0.1° or more using potassium bromide,[80, 81] and the impact of such magic angle deviations have been noted for proton detection of biomolecular samples.[82, 83] The proton line broadening present for even a small error in the magic angle prompted the use of methods to accurately adjust the magic angle directly using the sample of interest.[84, 85] A small deviation of about 0.025° from the magic angle (Fig. 7F) brings the amide proton to near perfect agreement with the measured value.

The linewidth becomes particularly sensitive to the magic angle in the fast spinning regime (Fig 7F). In this case a natural linewidth of only 16 Hz was assumed, which represents a spin echo applied on the channel, removing some hypothetical inhomogeneous contribution to the line. The simulations of Fig. 7 show that a misset of 0.05 ° results in more than a 10 percent increase in linewidth at 100 kHz MAS.

This observation led us to adjust the spinning angle for each sample according to the following procedure, which upon initial comparison yields similar results as obtained with J-modulated spectra for fully protonated samples.[85] First, the sample is spun to 100 kHz, and the variable temperature gas set to the desired value. Then only after the probe temperature is allowed to equilibrate for at least one hour is the angle adjusted in order to minimize the homogeneous component of the proton linewidth. In fully protonated membrane proteins, the homogeneous proton T2 (T2′) is typically 2 to 3 ms, such that a spin echo on the proton channel of about 3 ms retains sufficient sensitivity for optimization of the angle. We therefore adjusted the angle by maximizing the amide T2′ for the bulk proton signal, by insertion of a Hahn echo directly after the CP-HSQC. Typically, the relaxation delay (during the Hahn echo) was set to 3 ms, and 32 or 64 scans were needed at each step in the angle adjustment. The approach is similar to one based on scalar and dipolar oscillations.[85], except that in the T_2' method there are no signal oscillations allowing selection of any echo time.

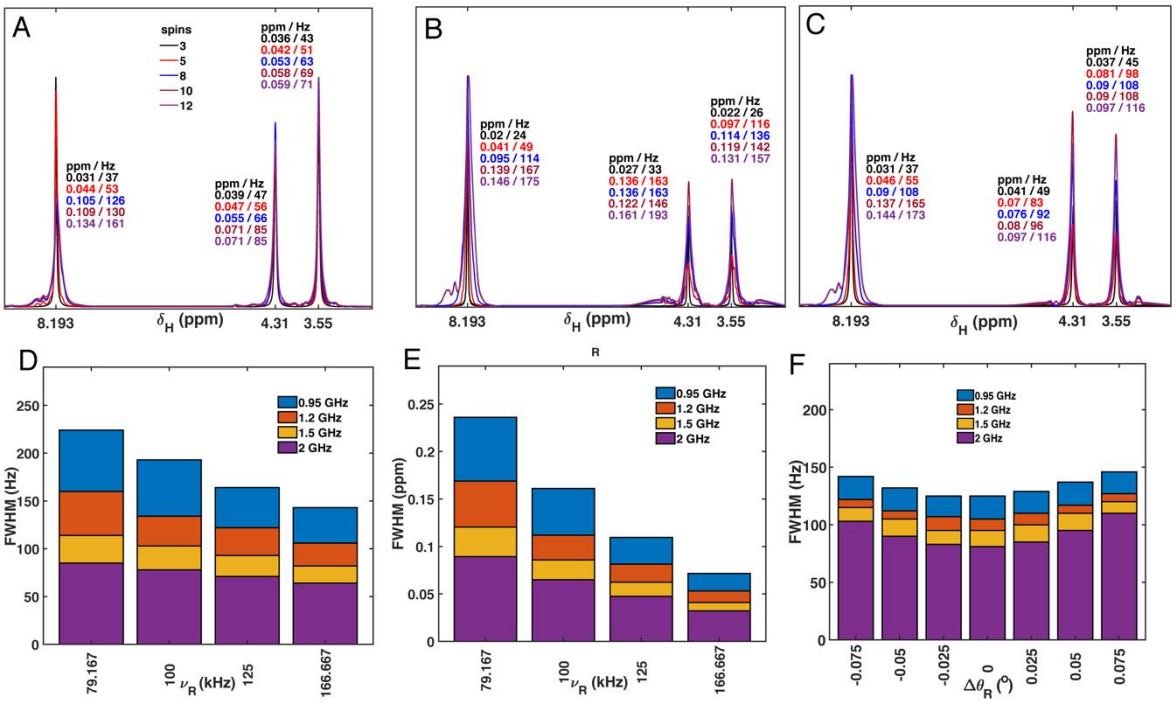

Figure 7. Simulated spectra of glycine protons, with different sets of spins included. The simulated spectra in A-C were for the 1.2 GHz magnet with 100 kHz MAS. In A, the closest 3 to 12 spins from pdb 2N70 were included stepwise (details in the SI). In B and C, two additional protons were added to fill a void near the G34 Hα protons. In B, these additional protons had chemical shift

offsets of 4.6 ppm, whereas in C, chemical shift offsets were set according to a DFT calculation (details in the SI). In D, the full linewidth at half max (FWHM) of the amide proton is shown for four fields and MAS frequencies, with units of Hz. 10 spins were simulated. In E, the same linewidths are shown in ppm. Panel F shows the sensitivity of the amide proton to magic angle misset. 10 spins were simulated at a spinning frequency of 100 kHz, for the indicated spectrometer frequencies. For A-E, 32 Hz Lorentzian line broadening was applied, and for F, 16 Hz was applied, since the panel represents the linewidth in a spin echo.

5. Conclusions

The improvement in sensitivity and resolution available with the 1.2 GHz spectrometer will broaden the applicability of the method or reduce the required instrument time. The theoretical sensitivity improvement alone of about 40 percent already leads to a two-fold time efficiency. On top of this effect, the improvement for a multi-dimensional dataset grows with the product of the improvement in each dimension. Three of the four membrane proteins we investigated here showed clear improvement in nitrogen linewidths measured in Hz, which are dominated by homogeneous effects, such that the resolution measured in ppm scales superlinearly with the ratio of magnetic fields. For protons the linewidth in Hz also improves. This means that for the typical 3D or 4D dataset required for analysis of complex protein spectra, taking a conservative 26% improvement (compared with a 950 MHz instrument) grows to an improvement that is better than a factor of 2 or better than 2.5, respectively. This is expected to result in a dramatic improvement in the ability of MAS NMR to address larger proteins, without the need for even higher spectral dimensions.

Supplementary Materials: The following are available online at www.mdpi.com/xxx/s1, Figure S1: The structural representation of 16 spins of Table S3 that were entered in linewidth simulations, Table S1: CP parameters for acquisition of the (H)CH and (H)NH spectra at 950 MHz spectrometer, Table S2: CP parameters for acquisition of the (H)CH and (H)NH spectra at 1200 MHz spectrometer Table S3: The set of spins used in the linewidth simulations.

Author Contributions: Conceptualization, L.B.A. and C.G.; methodology, L.B.A and E.N.; software, E.N.; investigation, K.T.M., X.Z., M.C.F., E.N., R.D., and K.X.; resources, S.B. and K.G; writing—original draft preparation, L.B.A.; writing—review and editing, E.N., K.T.M., X.Z., M.C.F., E.N., K.X., L.B.A., C.G., S.B., and R.D.; supervision, L.B.A.; project administration, L.B.A.; funding acquisition, C.G. and L.B.A.

Funding: This research was funded by the Deutsche Forschungsgemeinschaft, Emmy Noether grant number AN1316/1-1 and The APC was funded by AN1316/1-1. The 1.2 GHz instrument was funded by the Max Planck Society and the DFG and the Land Niedersachsen (76251-12-1/12) with the support of the BIN (center of biomoleculear imaging in neurodegeneration) board.

Conflicts of Interest: "The authors declare no conflict of interest." "The funders had no role in the design of the study; in the collection, analyses, or interpretation of data; in the writing of the manuscript, or in the decision to publish the results".

References

1. Bodenhausen, G.; Ruben, D. J., Natural abundance nitrogen-15 NMR by enhanced heteronuclear spectroscopy. *Chem. Phys. Lett.* **1980,** 69, (1), 185-189. https://doi.org/10.1016/0009-2614(80)80041-8
2. Ishii, Y.; Yesinowski, J. P.; Tycko, R., Sensitivity enhancement in solid-state (13)C NMR of synthetic polymers and biopolymers by (1)H NMR detection with high-speed magic angle spinning. *J. Am. Chem. Soc.* **2001,** 123, (12), 2921-2. 10.1021/ja015505j
3. Maricq, M. M.; Waugh, J. S., NMR in rotating solids. *J. Chem. Phys.* **1979,** 70, (7), 3300-3316. 10.1063/1.437915

4. Chevelkov, V.; Rehbein, K.; Diehl, A.; Reif, B., Ultrahigh resolution in proton solid-state NMR spectroscopy at high levels of deuteration. *Angew. Chem. Int. Ed. Engl.* **2006,** 45, (23), 3878-81. 10.1002/anie.200600328
5. Chevelkov, V.; van Rossum, B. J.; Castellani, F.; Rehbein, K.; Diehl, A.; Hohwy, M.; Steuernagel, S.; Engelke, F.; Oschkinat, H.; Reif, B., 1H detection in MAS solid-state NMR spectroscopy of biomacromolecules employing pulsed field gradients for residual solvent suppression. *J. Am. Chem. Soc.* **2003,** 125, (26), 7788-9. 10.1021/ja029354b
6. McDermott, A. E.; Creuzet, F. J.; Kolbert, A. C.; Griffin, R. G., High-resolution magic-angle-spinning NMR spectra of protons in deuterated solids. *J. Magn. Reson.* **1992,** 98, (2), 408-413. https://doi.org/10.1016/0022-2364(92)90141-S
7. Paulson, E. K.; Morcombe, C. R.; Gaponenko, V.; Dancheck, B.; Byrd, R. A.; Zilm, K. W., Sensitive High Resolution Inverse Detection NMR Spectroscopy of Proteins in the Solid State. *J. Am. Chem. Soc.* **2003,** 125, (51), 15831-15836. 10.1021/ja037315+
8. Reif, B.; Jaroniec, C. P.; Rienstra, C. M.; Hohwy, M.; Griffin, R. G., 1H–1H MAS Correlation Spectroscopy and Distance Measurements in a Deuterated Peptide. *J. Magn. Reson.* **2001,** 151, (2), 320-327. https://doi.org/10.1006/jmre.2001.2354
9. Zheng, L.; Fishbein, K. W.; Griffin, R. G.; Herzfeld, J., Two-dimensional solid-state proton NMR and proton exchange. *J. Am. Chem. Soc.* **1993,** 115, (14), 6254-6261. 10.1021/ja00067a045
10. Medeiros-Silva, J.; Mance, D.; Daniëls, M.; Jekhmane, S.; Houben, K.; Baldus, M.; Weingarth, M., 1H-Detected Solid-State NMR Studies of Water-Inaccessible Proteins In Vitro and In Situ. *Angew. Chem. Int. Ed. Engl.* **2016,** 55, (43), 13606-13610. https://doi.org/10.1002/anie.201606594
11. Ward, M. E.; Shi, L.; Lake, E.; Krishnamurthy, S.; Hutchins, H.; Brown, L. S.; Ladizhansky, V., Proton-Detected Solid-State NMR Reveals Intramembrane Polar Networks in a Seven-Helical Transmembrane Protein Proteorhodopsin. *J. Am. Chem. Soc.* **2011,** 133, (43), 17434-17443. 10.1021/ja207137h
12. Akbey, U.; Lange, S.; Trent Franks, W.; Linser, R.; Rehbein, K.; Diehl, A.; van Rossum, B. J.; Reif, B.; Oschkinat, H., Optimum levels of exchangeable protons in perdeuterated proteins for proton detection in MAS solid-state NMR spectroscopy. *J. Biomol. NMR* **2010,** 46, (1), 67-73. 10.1007/s10858-009-9369-0
13. Zhou, D. H.; Graesser, D. T.; Franks, W. T.; Rienstra, C. M., Sensitivity and resolution in proton solid-state NMR at intermediate deuteration levels: quantitative linewidth characterization and applications to correlation spectroscopy. *J. Magn. Reson.* **2006,** 178, (2), 297-307. 10.1016/j.jmr.2005.10.008
14. Samoson, A.; Tuherm, T.; Gan, Z., High-Field High-Speed MAS Resolution Enhancement in 1H NMR Spectroscopy of Solids. *Solid State Nucl. Magn. Reson.* **2001,** 20, (3), 130-136. https://doi.org/10.1006/snmr.2001.0037
15. Böckmann, A.; Ernst, M.; Meier, B. H., Spinning proteins, the faster, the better? *J. Magn. Reson.* **2015,** 253, 71-9. 10.1016/j.jmr.2015.01.012
16. Xue, K.; Sarkar, R.; Tosner, Z.; Lalli, D.; Motz, C.; Koch, B.; Pintacuda, G.; Reif, B., MAS dependent sensitivity of different isotopomers in selectively methyl protonated protein samples in solid state NMR. *J. Biomol. NMR* **2019,** 73, (10), 625-631. 10.1007/s10858-019-00274-0
17. Knight, M. J.; Webber, A. L.; Pell, A. J.; Guerry, P.; Barbet-Massin, E.; Bertini, I.; Felli, I. C.; Gonnelli, L.; Pierattelli, R.; Emsley, L.; Lesage, A.; Herrmann, T.; Pintacuda, G., Fast Resonance Assignment and Fold Determination of Human Superoxide Dismutase by High-Resolution Proton-Detected Solid-State MAS NMR Spectroscopy. *Angew. Chem. Int. Ed. Engl.* **2011,** 50, (49), 11697-11701. https://doi.org/10.1002/anie.201106340
18. Lewandowski, J. R.; Dumez, J.-N.; Akbey, Ü.; Lange, S.; Emsley, L.; Oschkinat, H., Enhanced Resolution and Coherence Lifetimes in the Solid-State NMR Spectroscopy of Perdeuterated Proteins under Ultrafast Magic-Angle Spinning. *J. Phys. Chem. Lett.* **2011,** 2, (17), 2205-2211. 10.1021/jz200844n
19. Agarwal, V.; Penzel, S.; Szekely, K.; Cadalbert, R.; Testori, E.; Oss, A.; Past, J.; Samoson, A.; Ernst, M.; Böckmann, A.; Meier, B. H., De novo 3D structure determination from sub-milligram protein samples by solid-state 100 kHz MAS NMR spectroscopy. *Angew. Chem. Int. Ed. Engl.* **2014,** 53, (45), 12253-6. 10.1002/anie.201405730

20. Barbet-Massin, E.; Pell, A. J.; Retel, J. S.; Andreas, L. B.; Jaudzems, K.; Franks, W. T.; Nieuwkoop, A. J.; Hiller, M.; Higman, V.; Guerry, P.; Bertarello, A.; Knight, M. J.; Felletti, M.; Le Marchand, T.; Kotelovica, S.; Akopjana, I.; Tars, K.; Stoppini, M.; Bellotti, V.; Bolognesi, M.; Ricagno, S.; Chou, J. J.; Griffin, R. G.; Oschkinat, H.; Lesage, A.; Emsley, L.; Herrmann, T.; Pintacuda, G., Rapid Proton-Detected NMR Assignment for Proteins with Fast Magic Angle Spinning. *J. Am. Chem. Soc.* **2014,** 136, (35), 12489-12497. 10.1021/ja507382j
21. Linser, R.; Dasari, M.; Hiller, M.; Higman, V.; Fink, U.; Lopez del Amo, J.-M.; Markovic, S.; Handel, L.; Kessler, B.; Schmieder, P.; Oesterhelt, D.; Oschkinat, H.; Reif, B., Proton-Detected Solid-State NMR Spectroscopy of Fibrillar and Membrane Proteins. *Angew. Chem. Int. Ed. Engl.* **2011,** 50, (19), 4508-4512. https://doi.org/10.1002/anie.201008244
22. Nieuwkoop, A. J.; Franks, W. T.; Rehbein, K.; Diehl, A.; Akbey, Ü.; Engelke, F.; Emsley, L.; Pintacuda, G.; Oschkinat, H., Sensitivity and resolution of proton detected spectra of a deuterated protein at 40 and 60 kHz magic-angle-spinning. *J. Biomol. NMR* **2015,** 61, (2), 161-171. 10.1007/s10858-015-9904-0
23. Andreas, L. B.; Le Marchand, T.; Jaudzems, K.; Pintacuda, G., High-resolution proton-detected NMR of proteins at very fast MAS. *J. Magn. Reson.* **2015,** 253, 36-49. 10.1016/j.jmr.2015.01.003
24. Penzel, S.; Oss, A.; Org, M.-L.; Samoson, A.; Böckmann, A.; Ernst, M.; Meier, B. H., Spinning faster: protein NMR at MAS frequencies up to 126 kHz. *J. Biomol. NMR* **2019,** 73, (1), 19-29. 10.1007/s10858-018-0219-9
25. Agarwal, V.; Reif, B., Residual methyl protonation in perdeuterated proteins for multi-dimensional correlation experiments in MAS solid-state NMR spectroscopy. *J. Magn. Reson.* **2008,** 194, (1), 16-24. 10.1016/j.jmr.2008.05.021
26. Agarwal, V.; Diehl, A.; Skrynnikov, N.; Reif, B., High Resolution 1H Detected 1H,13C Correlation Spectra in MAS Solid-State NMR using Deuterated Proteins with Selective 1H,2H Isotopic Labeling of Methyl Groups. *J. Am. Chem. Soc.* **2006,** 128, (39), 12620-12621. 10.1021/ja064379m
27. Asami, S.; Schmieder, P.; Reif, B., High resolution 1H-detected solid-state NMR spectroscopy of protein aliphatic resonances: access to tertiary structure information. *J. Am. Chem. Soc.* **2010,** 132, (43), 15133-5. 10.1021/ja106170h
28. Asami, S.; Szekely, K.; Schanda, P.; Meier, B. H.; Reif, B., Optimal degree of protonation for 1H detection of aliphatic sites in randomly deuterated proteins as a function of the MAS frequency. *J. Biomol. NMR* **2012,** 54, (2), 155-168. 10.1007/s10858-012-9659-9
29. Asami, S.; Porter, J. R.; Lange, O. F.; Reif, B., Access to Cα Backbone Dynamics of Biological Solids by 13C T1 Relaxation and Molecular Dynamics Simulation. *J. Am. Chem. Soc.* **2015,** 137, (3), 1094-1100. 10.1021/ja509367q
30. Mance, D.; Sinnige, T.; Kaplan, M.; Narasimhan, S.; Daniëls, M.; Houben, K.; Baldus, M.; Weingarth, M., An Efficient Labelling Approach to Harness Backbone and Side-Chain Protons in 1H-Detected Solid-State NMR Spectroscopy. *Angew. Chem. Int. Ed. Engl.* **2015,** 54, (52), 15799-15803. https://doi.org/10.1002/anie.201509170
31. Gardner, K. H.; Rosen, M. K.; Kay, L. E., Global folds of highly deuterated, methyl-protonated proteins by multidimensional NMR. *Biochemistry* **1997,** 36, (6), 1389-401. 10.1021/bi9624806
32. Goto, N. K.; Gardner, K. H.; Mueller, G. A.; Willis, R. C.; Kay, L. E., A robust and cost-effective method for the production of Val, Leu, Ile (delta 1) methyl-protonated 15N-, 13C-, 2H-labeled proteins. *J. Biomol. NMR* **1999,** 13, (4), 369-74. 10.1023/a:1008393201236
33. Gans, P.; Hamelin, O.; Sounier, R.; Ayala, I.; Durá, M. A.; Amero, C. D.; Noirclerc-Savoye, M.; Franzetti, B.; Plevin, M. J.; Boisbouvier, J., Stereospecific isotopic labeling of methyl groups for NMR spectroscopic studies of high-molecular-weight proteins. *Angew. Chem. Int. Ed. Engl.* **2010,** 49, (11), 1958-62. 10.1002/anie.200905660
34. Huber, M.; Hiller, S.; Schanda, P.; Ernst, M.; Böckmann, A.; Verel, R.; Meier, B. H., A Proton-Detected 4D Solid-State NMR Experiment for Protein Structure Determination. *ChemPhysChem* **2011,** 12, (5), 915-918. https://doi.org/10.1002/cphc.201100062
35. Kurauskas, V.; Crublet, E.; Macek, P.; Kerfah, R.; Gauto, D. F.; Boisbouvier, J.; Schanda, P., Sensitive proton-detected solid-state NMR spectroscopy of large proteins with selective CH3 labelling: application to the 50S ribosome subunit. *Chem. Commun.* **2016,** 52, (61), 9558-9561. 10.1039/C6CC04484K

36. Linser, R.; Bardiaux, B.; Higman, V.; Fink, U.; Reif, B., Structure calculation from unambiguous long-range amide and methyl 1H-1H distance restraints for a microcrystalline protein with MAS solid-state NMR spectroscopy. *J. Am. Chem. Soc.* **2011,** 133, (15), 5905-12. 10.1021/ja110222h
37. Takahashi, H.; Kainosho, M.; Akutsu, H.; Fujiwara, T., 1H-detected 1H-1H correlation spectroscopy of a stereo-array isotope labeled amino acid under fast magic-angle spinning. *J. Magn. Reson.* **2010,** 203, (2), 253-6. 10.1016/j.jmr.2010.01.005
38. Wang, S.; Parthasarathy, S.; Nishiyama, Y.; Endo, Y.; Nemoto, T.; Yamauchi, K.; Asakura, T.; Takeda, M.; Terauchi, T.; Kainosho, M.; Ishii, Y., Nano-mole scale side-chain signal assignment by 1H-detected protein solid-state NMR by ultra-fast magic-angle spinning and stereo-array isotope labeling. *PloS one* **2015,** 10, (4), e0122714. 10.1371/journal.pone.0122714
39. Movellan, K. T.; Najbauer, E. E.; Pratihar, S.; Salvi, M.; Giller, K.; Becker, S.; Andreas, L. B., Alpha protons as NMR probes in deuterated proteins. *J. Biomol. NMR* **2019,** 73, (1-2), 81-91. 10.1007/s10858-019-00230-y
40. Saxena, K.; Dutta, A.; Klein-Seetharaman, J.; Schwalbe, H., Isotope labeling in insect cells. *Methods Mol/ Biol.* **2012,** 831, 37-54. 10.1007/978-1-61779-480-3_3
41. Franke, B.; Opitz, C.; Isogai, S.; Grahl, A.; Delgado, L.; Gossert, A. D.; Grzesiek, S., Production of isotope-labeled proteins in insect cells for NMR. *J. Biomol. NMR* **2018,** 71, (3), 173-184. 10.1007/s10858-018-0172-7
42. Sastry, M.; Bewley, C. A.; Kwong, P. D., Mammalian expression of isotopically labeled proteins for NMR spectroscopy. *Adv. Exp. Med. Biol.* **2012,** 992, 197-211. 10.1007/978-94-007-4954-2_11
43. Zhou, D. H.; Shah, G.; Cormos, M.; Mullen, C.; Sandoz, D.; Rienstra, C. M., Proton-Detected Solid-State NMR Spectroscopy of Fully Protonated Proteins at 40 kHz Magic-Angle Spinning. *J. Am. Chem. Soc.* **2007,** 129, (38), 11791-11801. 10.1021/ja073462m
44. Marchetti, A.; Jehle, S.; Felletti, M.; Knight, M. J.; Wang, Y.; Xu, Z.-Q.; Park, A. Y.; Otting, G.; Lesage, A.; Emsley, L.; Dixon, N. E.; Pintacuda, G., Backbone Assignment of Fully Protonated Solid Proteins by 1H Detection and Ultrafast Magic-Angle-Spinning NMR Spectroscopy. *Angew. Chem. Int. Ed. Engl.* **2012,** 51, (43), 10756-10759. https://doi.org/10.1002/anie.201203124
45. Vasa, S. K.; Rovó, P.; Giller, K.; Becker, S.; Linser, R., Access to aliphatic protons as reporters in non-deuterated proteins by solid-state NMR. *Phys. Chem. Chem. Phys.* **2016,** 18, (12), 8359-8363. 10.1039/C5CP06601H
46. Mroue, K. H.; Nishiyama, Y.; Kumar Pandey, M.; Gong, B.; McNerny, E.; Kohn, D. H.; Morris, M. D.; Ramamoorthy, A., Proton-Detected Solid-State NMR Spectroscopy of Bone with Ultrafast Magic Angle Spinning. *Scie. Rep.* **2015,** 5, (1), 11991. 10.1038/srep11991
47. Nishiyama, Y., Fast magic-angle sample spinning solid-state NMR at 60-100kHz for natural abundance samples. *Solid State Nucl. Magn. Reson.* **2016,** 78, 24-36. 10.1016/j.ssnmr.2016.06.002
48. Pandey, M. K.; Nishiyama, Y., Determination of NH proton chemical shift anisotropy with 14N–1H heteronuclear decoupling using ultrafast magic angle spinning solid-state NMR. *J. Magn. Reson.* **2015,** 261, 133-140. https://doi.org/10.1016/j.jmr.2015.10.015
49. Andreas, L. B.; Jaudzems, K.; Stanek, J.; Lalli, D.; Bertarello, A.; Le Marchand, T.; Cala-De Paepe, D.; Kotelovica, S.; Akopjana, I.; Knott, B.; Wegner, S.; Engelke, F.; Lesage, A.; Emsley, L.; Tars, K.; Herrmann, T.; Pintacuda, G., Structure of fully protonated proteins by proton-detected magic-angle spinning NMR. *Proc. Natl. Acad. Sci. USA* **2016,** 113, (33), 9187. 10.1073/pnas.1602248113
50. Xue, K.; Sarkar, R.; Lalli, D.; Koch, B.; Pintacuda, G.; Tosner, Z.; Reif, B., Impact of Magnetic Field Strength on Resolution and Sensitivity of Proton Resonances in Biological Solids. *J. Phys. Chem. C* **2020,** 124, (41), 22631-22637. 10.1021/acs.jpcc.0c05407
51. Malär, A. A.; Smith-Penzel, S.; Camenisch, G.-M.; Wiegand, T.; Samoson, A.; Böckmann, A.; Ernst, M.; Meier, B. H., Quantifying proton NMR coherent linewidth in proteins under fast MAS conditions: a second moment approach. *Phys. Chem. Chem. Phys.* **2019,** 21, (35), 18850-18865. 10.1039/C9CP03414E

52. Butler, M. C.; Dumez, J.-N.; Emsley, L., Dynamics of large nuclear-spin systems from low-order correlations in Liouville space. *Chem. Phys. Lett.* **2009,** 477, (4), 377-381. https://doi.org/10.1016/j.cplett.2009.07.017
53. Kuprov, I.; Wagner-Rundell, N.; Hore, P. J., Polynomially scaling spin dynamics simulation algorithm based on adaptive state-space restriction. *J. Magn. Reson.* **2007,** 189, (2), 241-50. 10.1016/j.jmr.2007.09.014
54. Marion, D.; Gauto, D. F.; Ayala, I.; Giandoreggio-Barranco, K.; Schanda, P., Microsecond Protein Dynamics from Combined Bloch-McConnell and Near-Rotary-Resonance R1p Relaxation-Dispersion MAS NMR. *ChemPhysChem* **2019,** 20, (2), 276-284. https://doi.org/10.1002/cphc.201800935
55. Liang, B.; Tamm, L. K., NMR as a tool to investigate the structure, dynamics and function of membrane proteins. *Nat. Struct. Mol. Biol.* **2016,** 23, (6), 468-74. 10.1038/nsmb.3226
56. Linser, R.; Dasari, M.; Hiller, M.; Higman, V.; Fink, U.; Lopez del Amo, J. M.; Markovic, S.; Handel, L.; Kessler, B.; Schmieder, P.; Oesterhelt, D.; Oschkinat, H.; Reif, B., Proton-detected solid-state NMR spectroscopy of fibrillar and membrane proteins. *Angew. Chem. Int. Ed. Engl.* **2011,** 50, (19), 4508-12. 10.1002/anie.201008244
57. Zhou, D. H.; Rienstra, C. M., High-performance solvent suppression for proton detected solid-state NMR. *J. Magn. Reson.* **2008,** 192, (1), 167-172. 10.1016/j.jmr.2008.01.012
58. Lee, W.; Tonelli, M.; Markley, J. L., NMRFAM-SPARKY: enhanced software for biomolecular NMR spectroscopy. *Bioinformatics* **2014,** 31, (8), 1325-1327. 10.1093/bioinformatics/btu830
59. Najbauer, E. E.; Andreas, L. B., Correcting for magnetic field drift in magic-angle spinning NMR datasets. *J. Magn. Reson.* **2019,** 305, 1-4. 10.1016/j.jmr.2019.05.005
60. Andreas, L. B.; Eddy, M. T.; Pielak, R. M.; Chou, J.; Griffin, R. G., Magic Angle Spinning NMR Investigation of Influenza A M218–60: Support for an Allosteric Mechanism of Inhibition. *J. Am. Chem. Soc.* **2010,** 132, (32), 10958-10960. 10.1021/ja101537p
61. Salvi, M.; Schomburg, B.; Giller, K.; Graf, S.; Unden, G.; Becker, S.; Lange, A.; Griesinger, C., Sensory domain contraction in histidine kinase CitA triggers transmembrane signaling in the membrane-bound sensor. *Proc. Natl. Acad. Sci. USA* **2017,** 114, (12), 3115. 10.1073/pnas.1620286114
62. Eddy, M. T.; Andreas, L.; Teijido, O.; Su, Y.; Clark, L.; Noskov, S. Y.; Wagner, G.; Rostovtseva, T. K.; Griffin, R. G., Magic angle spinning nuclear magnetic resonance characterization of voltage-dependent anion channel gating in two-dimensional lipid crystalline bilayers. *Biochemistry* **2015,** 54, (4), 994-1005. 10.1021/bi501260r
63. Fox, D. A.; Larsson, P.; Lo, R. H.; Kroncke, B. M.; Kasson, P. M.; Columbus, L., Structure of the Neisserial Outer Membrane Protein Opa60: Loop Flexibility Essential to Receptor Recognition and Bacterial Engulfment. *J. Am. Chem. Soc.* **2014,** 136, (28), 9938-9946. 10.1021/ja503093y
64. Zhang, X. C.; Forster, M. C.; Nimerovsky, E.; Movellan, K. T.; Andreas, L. B., Transferred-Rotational-Echo Double Resonance. *J. Phys. Chem. A* **2021,** 125, (3), 754-769. 10.1021/acs.jpca.0c09033
65. Ernst, R. R.; Bodenhausen, G.; Wokaun, A., *Principles of Nuclear Magnetic Resonance in One and Two Dimensions*. Clarendon Press: Oxford, 1987.
66. Nimerovsky, E.; Goldbourt, A., Insights into the spin dynamics of a large anisotropy spin subjected to long-pulse irradiation under a modified REDOR experiment. *J. Magn. Reson.* **2012,** 225, 130-141. https://doi.org/10.1016/j.jmr.2012.09.015
67. Hou, G.; Byeon, I.-J. L.; Ahn, J.; Gronenborn, A. M.; Polenova, T., 1H–13C/1H–15N Heteronuclear Dipolar Recoupling by R-Symmetry Sequences Under Fast Magic Angle Spinning for Dynamics Analysis of Biological and Organic Solids. *J. Am. Chem. Soc.* **2011,** 133, (46), 18646-18655. 10.1021/ja203771a
68. Frisch, M. J.; Trucks, G. W.; Schlegel, H. B.; Scuseria, G. E.; Robb, M. A.; Cheeseman, J. R.; Scalmani, G.; Barone, V.; Petersson, G. A.; Nakatsuji, H.; Li, X.; Caricato, M.; Marenich, A. V.; Bloino, J.; Janesko, B. G.; Gomperts, R.; Mennucci, B.; Hratchian, H. P.; Ortiz, J. V.; Izmaylov, A. F.; Sonnenberg, J. L.; Williams; Ding, F.; Lipparini, F.; Egidi, F.; Goings, J.; Peng, B.; Petrone, A.; Henderson, T.; Ranasinghe, D.; Zakrzewski, V. G.; Gao, J.; Rega, N.; Zheng, G.; Liang, W.; Hada, M.; Ehara,

M.; Toyota, K.; Fukuda, R.; Hasegawa, J.; Ishida, M.; Nakajima, T.; Honda, Y.; Kitao, O.; Nakai, H.; Vreven, T.; Throssell, K.; Montgomery Jr., J. A.; Peralta, J. E.; Ogliaro, F.; Bearpark, M. J.; Heyd, J. J.; Brothers, E. N.; Kudin, K. N.; Staroverov, V. N.; Keith, T. A.; Kobayashi, R.; Normand, J.; Raghavachari, K.; Rendell, A. P.; Burant, J. C.; Iyengar, S. S.; Tomasi, J.; Cossi, M.; Millam, J. M.; Klene, M.; Adamo, C.; Cammi, R.; Ochterski, J. W.; Martin, R. L.; Morokuma, K.; Farkas, O.; Foresman, J. B.; Fox, D. J. *Gaussian 16 Rev. C.01*, Wallingford, CT, 2016.

69. Gauss, J., Effects of electron correlation in the calculation of nuclear magnetic resonance chemical shifts. *J. Chem. Phys.* **1993,** 99, (5), 3629-3643. 10.1063/1.466161
70. Roothaan, C. C. J., New Developments in Molecular Orbital Theory. *Rev. Mod. Phys.* **1951,** 23, (2), 69-89. 10.1103/RevModPhys.23.69
71. Stewart, J. J. P., Optimization of parameters for semiempirical methods V: Modification of NDDO approximations and application to 70 elements. *J. Mol. Mod.* **2007,** 13, (12), 1173-1213. 10.1007/s00894-007-0233-4
72. Becke, A. D., Density-functional thermochemistry. III. The role of exact exchange. *J. Chem. Phys.* **1993,** 98, (7), 5648-5652. 10.1063/1.464913
73. Wang, C.; Takeuchi, K.; Pinto, L. H.; Lamb, R. A., Ion channel activity of influenza A virus M2 protein: characterization of the amantadine block. *J. virol.* **1993,** 67, (9), 5585-5594. 10.1128/JVI.67.9.5585-5594.1993
74. Bright, R. A.; Shay, D. K.; Shu, B.; Cox, N. J.; Klimov, A. I., Adamantane Resistance Among Influenza A Viruses Isolated Early During the 2005-2006 Influenza Season in the United States. *JAMA* **2006,** 295, (8), 891-894. 10.1001/jama.295.8.joc60020
75. Eddy, M. T.; Su, Y.; Silvers, R.; Andreas, L.; Clark, L.; Wagner, G.; Pintacuda, G.; Emsley, L.; Griffin, R. G., Lipid bilayer-bound conformation of an integral membrane beta barrel protein by multidimensional MAS NMR. *J. Biomol. NMR* **2015,** 61, (3-4), 299-310. 10.1007/s10858-015-9903-1
76. Malorny, B.; Morelli, G.; Kusecek, B.; Kolberg, J.; Achtman, M., Sequence diversity, predicted two-dimensional protein structure, and epitope mapping of neisserial Opa proteins. *J. Bacteriol.* **1998,** 180, (5), 1323-30. 10.1128/jb.180.5.1323-1330.1998
77. Hauck, C. R.; Meyer, T. F., 'Small' talk: Opa proteins as mediators of Neisseria–host-cell communication. *Curr. Opin. Microbiol.* **2003,** 6, (1), 43-49. https://doi.org/10.1016/S1369-5274(03)00004-3
78. Bos, M. P.; Kao, D.; Hogan, D. M.; Grant, C. C. R.; Belland, R. J., Carcinoembryonic Antigen Family Receptor Recognition by Gonococcal Opa Proteins Requires Distinct Combinations of Hypervariable Opa Protein Domains. *Infect. Immun.* **2002,** 70, (4), 1715-1723. 10.1128/iai.70.4.1715-1723.2002
79. Xue, K.; Sarkar, R.; Motz, C.; Asami, S.; Decker, V.; Wegner, S.; Tosner, Z.; Reif, B., Magic-Angle Spinning Frequencies beyond 300 kHz Are Necessary To Yield Maximum Sensitivity in Selectively Methyl Protonated Protein Samples in Solid-State NMR. *J. Phys. Chem. C* **2018,** 122, (28), 16437-16442. 10.1021/acs.jpcc.8b05600
80. Sarkar, R.; Rodriguez Camargo, D. C.; Pintacuda, G.; Reif, B., Restoring Resolution in Biological Solid-State NMR under Conditions of Off-Magic-Angle Spinning. *J. Phys. Chem. Lett.* **2015,** 6, (24), 5040-5044. 10.1021/acs.jpclett.5b02467
81. Frye, J. S.; Maciel, G. E., Setting the magic angle using a quadrupolar nuclide. *J. of Magn. Reson. (1969)* **1982,** 48, (1), 125-131. https://doi.org/10.1016/0022-2364(82)90243-8
82. Xue, K.; Mühlbauer, M.; Mamone, S.; Sarkar, R.; Reif, B., Accurate Determination of 1H-15N Dipolar Couplings Using Inaccurate Settings of the Magic Angle in Solid-State NMR Spectroscopy. *Angew. Chem. Int. Ed. Engl.* **2019,** 58, (13), 4286-4290. https://doi.org/10.1002/anie.201814314
83. Xue, K.; Mamone, S.; Koch, B.; Sarkar, R.; Reif, B., Determination of methyl order parameters using solid state NMR under off magic angle spinning. *J. Biomol. NMR* **2019,** 73, (8), 471-475. 10.1007/s10858-019-00253-5
84. Pileio, G.; Guo, Y.; Pham, T. N.; Griffin, J. M.; Levitt, M. H.; Brown, S. P., Residual Dipolar Couplings by Off-Magic-Angle Spinning in Solid-State Nuclear Magnetic Resonance Spectroscopy. *J. Am. Chem. Soc.* **2007,** 129, (36), 10972-10973. 10.1021/ja0721115

85. Penzel, S.; Smith, A. A.; Ernst, M.; Meier, B. H., Setting the magic angle for fast magic-angle spinning probes. *J. Magn. Reson.* **2018,** 293, 115-122. https://doi.org/10.1016/j.jmr.2018.06.002